Photoisomerization of *trans*-Stilbene in Moderately Compressed Gases: Pressure-Dependent Effective Barriers

A. Meyer,[†] J. Schroeder,[†,‡] and J. Troe*[,†,‡]

Institut für Physikalische Chemie, Universität Göttingen, Tammannstrasse 6, D-37077 Göttingen, Germany, and Abteilung für Spektroskopie und Photochemische Kinetik, Max-Planck-Institut für Biophysikalische Chemie, Am Fassberg, D-37077 Göttingen, Germany

Received: August 3, 1999; In Final Form: October 1, 1999

A systematic experimental study of the bath gas and pressure dependence of the photoisomerization of *trans*-stilbene in the low to intermediate pressure regime is presented. The analysis of the results by a detailed numerical master equation simulation reveals specific bath gas influences in the effective specific rate constants for isomerization that are already observable at pressures of about 1 bar. The low-pressure regime of the unimolecular reaction in the S_1 state can be located in the pressure range well below 1 bar for most of the bath gases. The effective "high-pressure limit" of the photoisomerization rate constant that can be extracted from the simulation is found to be pressure dependent, approaching a bath gas specific plateau value in the 10 bar range for bath gases such as methane, ethane, propane, or xenon. The existence of a bath gas dependent plateau of the effective high-pressure limit is consistent with the proposition of a pressure- or density-dependent effective barrier of the reaction. The values obtained for the pressure-dependent barrier height agree with the trend observed in earlier experiments in highly compressed gases and liquids and confirm a substantial contribution of "static" lowering of the reaction barrier. Additional "dynamic" lowering of the effectice barrier due to collision-induced intramolecular vibrational energy redistribution cannot be ruled out, however, and the relative importance of these two contributions remains an open question. The recently proposed effect of vibrational Franck−Condon cooling upon optical excitation of *trans*-stilbene definitely is not consistent with the experimental results.

Introduction

The influence of fluid solvents on the kinetics and the dynamics of elementary chemical processes such as unimolecular fragmentation, rearrangement, or recombination reactions at present is the subject of extensive experimental and theoretical research efforts. These investigations have led to considerable progress in the description of the fundamental phenomena involved. Nevertheless, it is still difficult to develop general physical models of reactions in solution because several complicated phenomena have to be taken into account simultaneously, such as collisional energy transfer between reactant and solvent molecules, solvent-induced intramolecular vibrational energy redistribution (IVR), solvation shell structure, solvent-induced changes of the potential energy surface (PES), solvation dynamics, and microscopic- and frequency-dependent friction. Obviously, the relative significance of these contributions varies with the solvent environment, in particular with its density, when the time scales for competing and interrelated processes change relative to each other. Therefore, as a prerequisite for a quantitative understanding of such reactions one has to try to disentangle these processes as much as possible.

One promising way to achieve the goal of separating the processes involved is the systematic variation of the solvent density, starting from isolated molecule conditions in a supersonic beam expansion or in a low pressure gas, and then gradually increasing the complexity of the environment toward common liquid solution conditions. In this manner, the reaction proceeds from a purely intramolecular process via the domain of isolated binary collision events or pair interactions toward multiple interactions in a supercritical fluid and the diffusive regime in liquid solvents. Along this route, the dynamics is expected to become increasingly complex, but in each density regime certain characteristic processes dominate which may be identified and to a certain extent studied separately.

In this paper we focus attention on the transition from low to intermediate gas pressure where densities are just sufficiently high that local excess densities of the solvent in the vicinity of the reacting solute become significant. As an example, we investigate the solvent influence on the trans−cis photoisomerization of *trans*-stilbene, a unimolecular reaction on the S_1 potential energy surface which has been studied extensively and which has served as a model system for barrier crossing processes. The interpretation of the pressure dependence of the rate coefficient of this reaction is still the subject of controversial discussions, calling for more detailed systematic investigations of the solvent influence in particular. As a number of excellent and comprehensive reviews on this type of reaction are available, covering aspects of classical photochemistry[1−3] as well as picosecond dynamics and reaction kinetics,[4−8] we only briefly summarize the main points that are relevant for this study.

The photoisomerization of *trans*-stilbene has been investigated before under a variety of physical conditions. The observed dependence of the rate coefficient in liquid solution on temperature, pressure, and solvent has been discussed in terms of frequency-dependent friction,[9−11] multidimensionality of the potential energy surface,[12−14] breakdown of the Stokes−Einstein relation,[15,16] and solvent-induced changes of the height and shape of the effective potential barrier in the singlet excited state.[17,18] In suggesting the latter model we assumed that the effective

10.1021/jp992747l CCC: $18.00 © 1999 American Chemical Society
Published on Web 11/10/1999

height E_0 of the barrier of reaction decreases due to "static solute−solvent interactions" as the solvent density increases from low-pressure gas to liquid-phase values. As we pointed out,[19] these barrier effects should also be observable in jet-cooled isolated solute−solvent clusters as the solvation shell gradually closes around the solute. Recent measurements of jet-cooled *trans*-stilbene-*n*-hexane, (1:*n*)-clusters, $n = 1-5$, have provided new insight into this problem.[20] Picosecond pump−probe measurements with resonance-enhanced two-photon ionization (R2PI-probe) and time-of-flight (TOF) mass resolved detection showed that the decrease of the *trans*-stilbene S_1 lifetime with increasing excitation energy becomes less pronounced as the size of the clusters increases. It was argued that this surprising influence of microscopic solvation on the isomerization rate coefficients is related to higher internal solute−solvent friction in the cluster. Furthermore, there were also indications that, in the (1:1)-complex, the barrier to isomerization was about 20% lower than in isolated *trans*-stilbene, while it seemed to increase again as the number of *n*-hexane molecules in the cluster became larger. On the other hand, fluorescence lifetime measurements on jet-cooled 1:1 *trans*-stilbene-*n*-hexane clusters give a clear indication that the effective barrier E_0 in the complex is lower than in the isolated molecule by about 20%.[21]

Since the question of a lowering of the effective barrier for reaction by clustering remained open after the beam experiments, in the present work we are undertaking a new approach by studying the reaction in a series of bath gases from the low to the medium-pressure gas-phase regime. If one compares the thermal isomerization rate coefficient in medium-pressure gases with the corresponding high-pressure limit k_∞, such as calculated from microcanonical rate coefficients $k(E)$ of jet-cooled isolated *trans*-stilbene, one finds an order of magnitude discrepancy.[22] The present type of experiments in conjunction with numerical master equation simulations such as described below should characterize the "high-pressure limit k_∞" in a more detailed way than was the case in earlier studies.[23−25]

So far, the discussion of the puzzling discrepancy between measured and calculated k_∞ has focused on two points: (I) the applicability of statistical rate theory to the reaction under collision-free or low-pressure conditions and (II) the properties of the excited state PES for this reaction. The former concerns the role of incomplete IVR in the isolated molecule, possibly acting as a bottleneck, in contrast to the situation in solution where efficient collision-induced IVR in solution might rapidly lead to a statistical energy distribution among the solute vibrational modes, such that the observed rate is the "correct thermal" reaction rate.[22,23] On the other hand, the lack of reliable knowledge about the PES has led to interpretations involving (II/i) a diabatic PES causing a high degree of nonadiabaticity of the dynamics in the isolated molecule which is reduced as solvent friction slows down passage through the potential curve crossing region,[26] (II/ii) an adiabatic PES affected by "static" solute−solvent interactions that reduce the effective energy barrier E_0 in the low-density fluid,[18,25] and (II/iii) an adiabatic PES based on an improved model of *trans*-stilbene for statistical rate theory calculations and the assumption of vibrational Franck−Condon cooling of *trans*-stilbene upon electronic excitation to the S_1 state.[27]

All models except model (II/ii) consider nonspecific influences of the solvent on the reaction, i.e., the increase in collision rate with rising density to be responsible for collision induced IVR (I), enhancement of surface crossing rates (II/i), or rapid equilibration of the vibrational temperature after initial vibrational cooling by the light absorption process (II/iii). Consequently, these models predict a solvent-independent statistical high-pressure limit of the rate constant. In contrast to the models (I), (II/i), and (II/iii), model (II/ii) leads to the expectation that k_∞ depends on solvent properties such as polarizability or polarity. The corresponding effects in the reaction rate coefficient should be observable in the regime between isolated *trans*-stilbene and fluid solvent densities corresponding to bath gas pressures in the range between 10^{-1} bar and 10^2 bar. This is the falloff regime of the unimolecular photoisomerization reaction of *trans*-stilbene in the S_1 state and it is located well below the densities of the so-called Kramers turnover region which was investigated in great detail in the past.[14,18,28−32]

Whereas determinations of microcanonical rate coefficients $k(E)$ from supersonic jets,[21,23,24,33−36] fluorescence decay measurements under thermal collision-free conditions,[37−40] and studies of the density dependence of the photoisomerization rate coefficients at bath gas pressures above 5−10 bar in different solvents are available,[18,28,29,31,35,41] systematic studies at lower pressure are scarce.[39,40] As one may expect to find essential clues to the discussed problem in this density regime, we investigated *trans*-stilbene fluorescence decays in a variety of fluid solvents in the relevant pressure range in great detail. The analysis of the observed decays required a complete master equation simulation, taking into account the details of collisional energy transfer to the solvent environment.[40]

Experimental Section

Fluorescence decays of *trans*-stilbene after laser excitation at 310.4 nm were measured with a standard single photon counting system described in more detail elsewhere.[21,40] Stilbene crystals were introduced into the heated stainless steel sample cell shown in Figure 1 such that the concentration was determined by the vapor pressure of stilbene of about 10 μbar. The cell could be evacuated to pressures below 50 μbar, and its temperature was controlled to within 0.5 °C between 20 °C and 100 °C. Various bath gases were introduced, pressures above 1 bar being measured with a mechanical manometer (WIKA Kl. 0.6, 0−25 bar), while a piezoelectric manometer (Sensotec, A-5 8246−38) was used up to 1 bar.

The experimental setup is shown in Figure 2. The excitation light source was a synchronously pumped dye-laser (Coherent model 720) driven at a repetition rate of 76 MHz by an actively mode locked Nd:YLF laser (Coherent Antares 76S). As laser dye we used DCM Spezial (LambdaChrome 6501) to obtain pulses of 2 ps duration and 2.5 nJ energy at a wavelength of 620.8 nm. The pulses were frequency doubled in a $LiIO_3$ crystal of 6 mm length, the fundamental was blocked with a glass filter (Schott UG11), and the UV pulses were slightly focused ($f =$ 200 mm) into the sample cell while fluorescence perpendicular to the direction of propagation of the exciting laser beam was collected by a collimating lens and focused onto the detector window. To reduce reflection of the excitation light onto the detector, the interior of the sample cell was optically shielded from the observation window by a baffle system (Figure 1). Stray light from the excitation beam was blocked by a glass filter (Schott WG335) in front of the detector. Care was taken that emission from the entire fluorescence band of stilbene reached the photomultiplier cathode.

As detector, we employed a fast microchannel plate photomultiplier (MCP, Hamamatsu model R3809U) operated at −2.9 kV and kept at −5 °C to reduce the dark count rate to 2−4 Hz. Its output pulses were amplified in a preamplifier of 1.5 GHz bandwidth and 36 dB gain (Hamamatsu C5594), passively delayed and fed into a constant fraction discriminator (CFD,

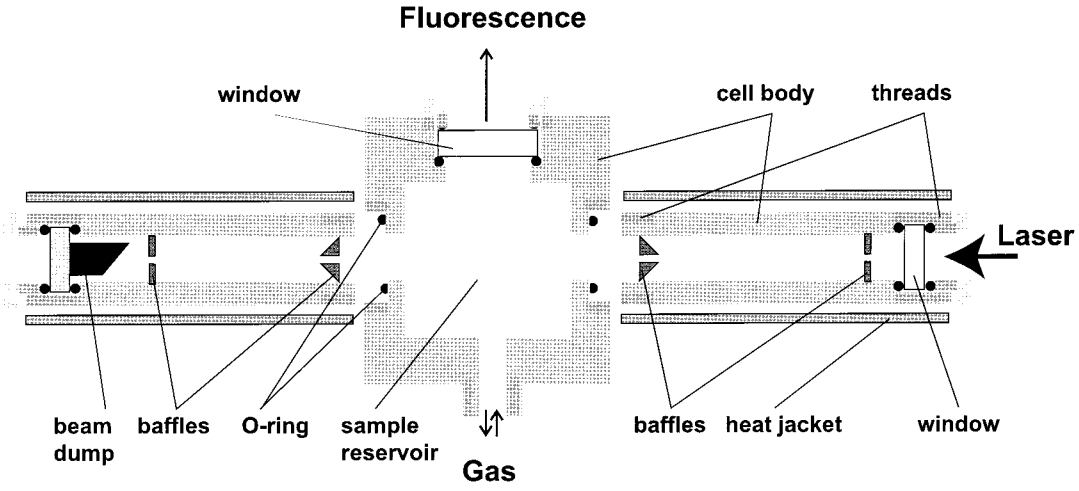

Figure 1. Sample cell used for fluorescence measurements at pressures between 50 μbar and 40 bar.

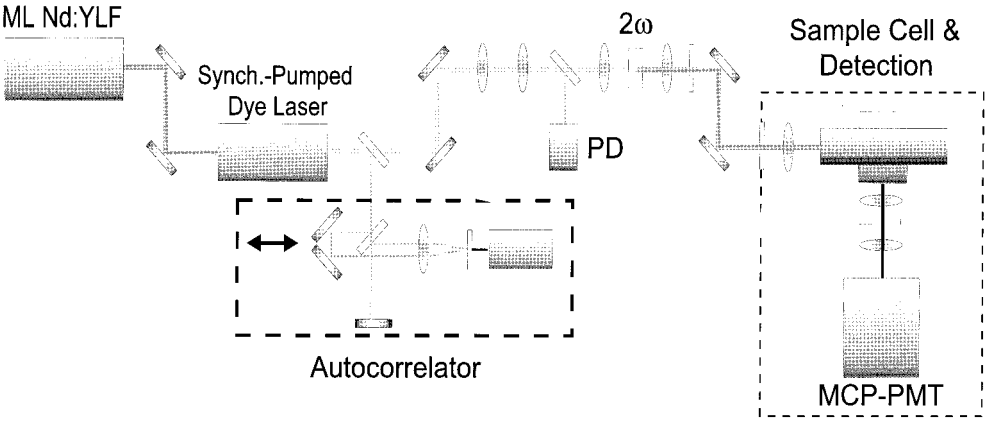

Figure 2. Experimental setup showing laser excitation and single photon counting detection.

Tennelec 454) to generate the start signals for a time-to-amplitude converter (TAC, Canberra 862) operated in reverse mode. Stop signals were derived from a second CFD triggered by a fast photodiode monitoring the train of laser excitation pulses. The TAC output was digitized in a Wilkinson type converter (Nuclear Data/Canberra 8713; 4096 channels) and finally registered and analyzed in a computer. In the operating setup we employed a temporal channel width of 7.1 ps. The overall instrument response function had a fwhm of 30 ps giving a time resolution of better than 20 ps after signal deconvolution, the spectral bandwidth of the excitation pulses at 310.4 nm was 0.5 nm.[36]

We used HPLC purified *trans*-stilbene in our experiments, while the bath gases were used as supplied by Messer-Griesheim: He (99.996%), Ne (99.995%), Ar (99.998%), Xe (99.998%), CH_4 (99.995%), C_2H_6 (99.95%), C_3H_8 (99.95%), N_2 (99.996%), and CO_2 (99.995%).

Results

The fluorescence decay measured in pure *trans*-stilbene vapor under collision-free conditions is nonexponential such as demonstrated in Figure 3 for an excitation wavelength of λ_{exc} = 310.4 nm and a sample temperature of 323 K. The excitation energy is close to the energy E_0^0 of the 0−0 transition as determined for the jet-cooled molecule corresponding to a wavelength of 310.23 nm. The shape of the fluorescence decay curve reflects the temporal evolution of the initial population distribution $g(E,t = 0)$ in the S_1 state created by exciting a thermal ensemble of ground state *trans*-stilbene molecules with a monochromatic laser pulse (E denotes the energy in the S_1 state, i.e., $E = E_{total} - E_0^0$). Molecules with energy E greater than the energy barrier E_0 in the S_1 state decay with a rate constant $k_f(E) = k_{rad} + k(E)$ where k_{rad} and $k(E)$ denote the radiative and the energy dependent nonradiative photoisomerization rate constant of *trans*-stilbene in the S_1 state, respectively. The energy dependence of $k(E)$ gives rise to the observed nonexponential decay of the fluorescence according to

$$c(t) = c_0 \int_0^\infty g(E,t) \exp(-k_f(E)t)\, dE \qquad (1)$$

where $c(t)$ and c_0 are the concentration of molecules in the S_1 state at time t and $t = 0$, respectively, and $g(E,t)$ is the energy distribution at time t.

When a buffer gas is added, the time evolution of $c(t)$ and $g(E,t)$ in addition is determined by energy transfer in collisions with solvent molecules. Fluorescence decay raw data shown in Figures 4 and 5 obtained in the rare gases He, Ne, Ar, Xe and in the alkanes CH_4, C_2H_6, C_3H_6, as well as CO_2, at a temperature of 323 K and various pressures, illustrate the persisting nonexponential character of the decays and the increase of the decay rate with pressure. The initial nonexponential parts of the decays are characterized by the evolution of the initial distribution $g(E,t=0)$ toward a stationary distribution $g'(E)$. The initial period becomes shorter with increasing pressure. After the initial period the stationary distribution decays exponentially with the first-order rate constant k_{iso}. In the high-pressure limit $g'(E)$ equals the equilibrium distribution $f(E)$, and k_{iso} becomes k_∞. Inspecting the figures, it is also evident that, at constant

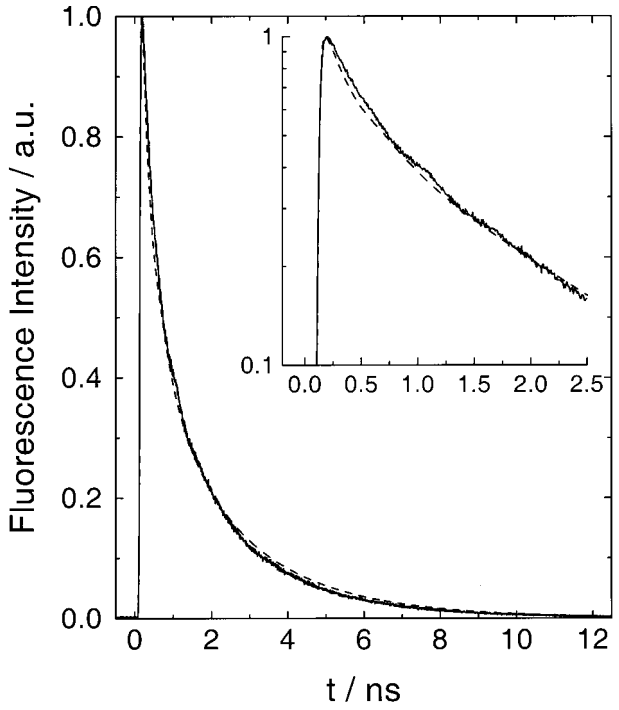

Figure 3. Fluorescence decay of *trans*-stilbene vapor at 323 K under collision-free conditions after excitation at 310.4 nm: measured trace (full line) and RRKM fit using the Warshel−Troe harmonic frequencies for *trans*-stilbene and the transition state and a thermal vibrational distribution in the S_1 state as initial distribution $g(E,t=0)$ (dashed line; see text). The inset shows the initial nonexponential period of the decay in a semilogarithmic plot. After about 2 ns the decay becomes exponential with a time constant corresponding to the radiative lifetime of *trans*-stilbene in the S_1 state.

pressure, the decays are faster for more complex solvents having a higher polarizability.

Before going into a more detailed analysis in the next section, as a first approximation one may ignore the nonexponential initial period and analyze the single-exponential decay at longer times which leads to the first-order fluorescence decay rate constants k_f. After subtracting the radiative rate constant[33] $k_{rad} = 3.7 \times 10^8\ s^{-1}$ one obtains values of $k_{iso} = k_f - k_{rad}$ which may be compared with values reported earlier for ethane at 350 K[31] and methane at 296 K.[39,41] (A density-independent value of k_{rad} can be used here, because variations due to changes in the refractive index of the solvent in this pressure range are less than 2%.[14,42]) Figure 6 demonstrates that, allowing for the temperature dependence of k_{iso}, the decay rate constants obtained from this type of single-exponential analysis agree with results of previous fluorescence decay measurements.[31,39] It is also evident from the density dependence of the fluorescence decay rates in Figure 6 that a decrease of k_{iso} due to solvent friction is observed only at higher densities beyond the range investigated in the present study.

Numerical Modeling

Specific Rate Constants $k(E)$. As discussed previously,[25] the energy dependence of $k(E)$ measured in supersonic expansions[21,23,24,33−36] can be fit by an RRKM model using the threshold energy E_0 and one frequency scaling factor as adjustable parameters

$$k(E) = \frac{W^{\neq}(E - E_0)}{h\rho(E)} \qquad (2)$$

Here the numerator is given by the number of states up to energy E in the transition state, h is Planck's constant and $\rho(E)$ is the reactant density of states. It has to be calculated using a set of vibrational frequencies for *trans*-stilbene in the S_1 state and the transition state employing direct counting with the Beyer−Swinehart algorithm.[43,44]

Taking the Negri−Orlandi model B (adiabatic transition state)[45] with a frequency of 56 cm^{-1} for the reaction coordinate and taking $E_0 = 1250\ cm^{-1}$ gives fair agreement of calculated $k(E)$ values with experimental lifetime data. The fit can be improved by optimizing the RRKM model following an approach proposed by Troe,[25] who suggested a common scaling factor F for adjusting a subset of the activated complex frequencies. Using $F = 1.05$ for all frequencies which presumably involve motion of the ethylenic double bond, i.e., oscillators at 57, 65, 177, 272, 315, 455, 478, 713, 765, 870, 1170, 1234, 1235, 1303, and 1598 cm^{-1}, yields a fitted value of $E_0 = (1260 \pm 50)\ cm^{-1}$. Still, at excess energies below 1300 cm^{-1} this model slightly underestimates the rate coefficients $k(E)$. Possible explanations for this discrepancy have been discussed in detail elsewhere.[21] The two models practically give the same value of $k_\infty = (4.1 \pm 0.1) \times 10^9\ s^{-1}$ at 323 K.

Initial Distribution. The initial distribution $g(E,t=0)$ determines the early part of the fluorescence decay. For a large polyatomic molecule like *trans*-stilbene having a comparatively high density of states one may assume that under the experimental conditions ($T = 323$ K) Franck−Condon factors do not vary significantly with vibrational state as vibrational frequencies do not differ extensively between the S_0 and S_1 electronic states. In this case, no Franck−Condon shaping of the population takes place and monochromatic laser excitation of the 0−0 transition carries the ground state thermal distribution $f(E)$ into the S_1 state essentially without distortion. The validity of this assumption can be tested by modeling concentration time profiles of the isomerization reaction under collision-free conditions according to eq 1. Figure 3 shows an experimentally recorded fluorescence decay curve for *trans*-stilbene excited into the origin of the S_0−S_1 transition under collision-free conditions and the result of a simulation on the basis of eqs 1 and 2 with $k(E)$ and $\rho(E)$ as determined in the preceding section, and a thermal energy distribution at $T = 323$ K for the initial distribution. In other words,

$$g(E,t=0) = f(E) = \frac{\rho(E)\exp(-E/k_BT)}{\int_0^\infty \rho(E)\exp(-E/k_BT)\,dE} \qquad (3)$$

Taking into account the fact that no fit parameters are used, good agreement with experiment is obtained. This shows that assuming a ground state vibrational equilibrium population for $g(E,t=0)$ with a mean energy $\langle E\rangle_0 \approx 2200\ cm^{-1}$ at $T = 323$ K is a reasonable assumption. In contrast to the earlier work by Fleming and co-workers,[39] we do not find that including the rotational contribution in the density of states leads to an improvement of the fit. It has to be taken into account, however, that our experiments were performed at a temperature of 50 °C while Fleming and co-workers measured at room temperature.

Master Equation. The initial period of the fluorescence decays, with a gradual evolution of the distribution from that reached by optical excitation toward steady state requires a detailed analysis that takes into account both $k(E)$ and collisional energy transfer in binary collisions with the bath gas. Considering densities of states of *trans*-stilbene in the S_1 state of $2 \times 10^5/cm^{-1}$ at $\langle E\rangle_0 = 2200\ cm^{-1}$ and $3 \times 10^2/cm^{-1}$ at $E_0 = 1260\ cm^{-1}$, we can use a continuous master equation description to model the detailed kinetics of energy transfer

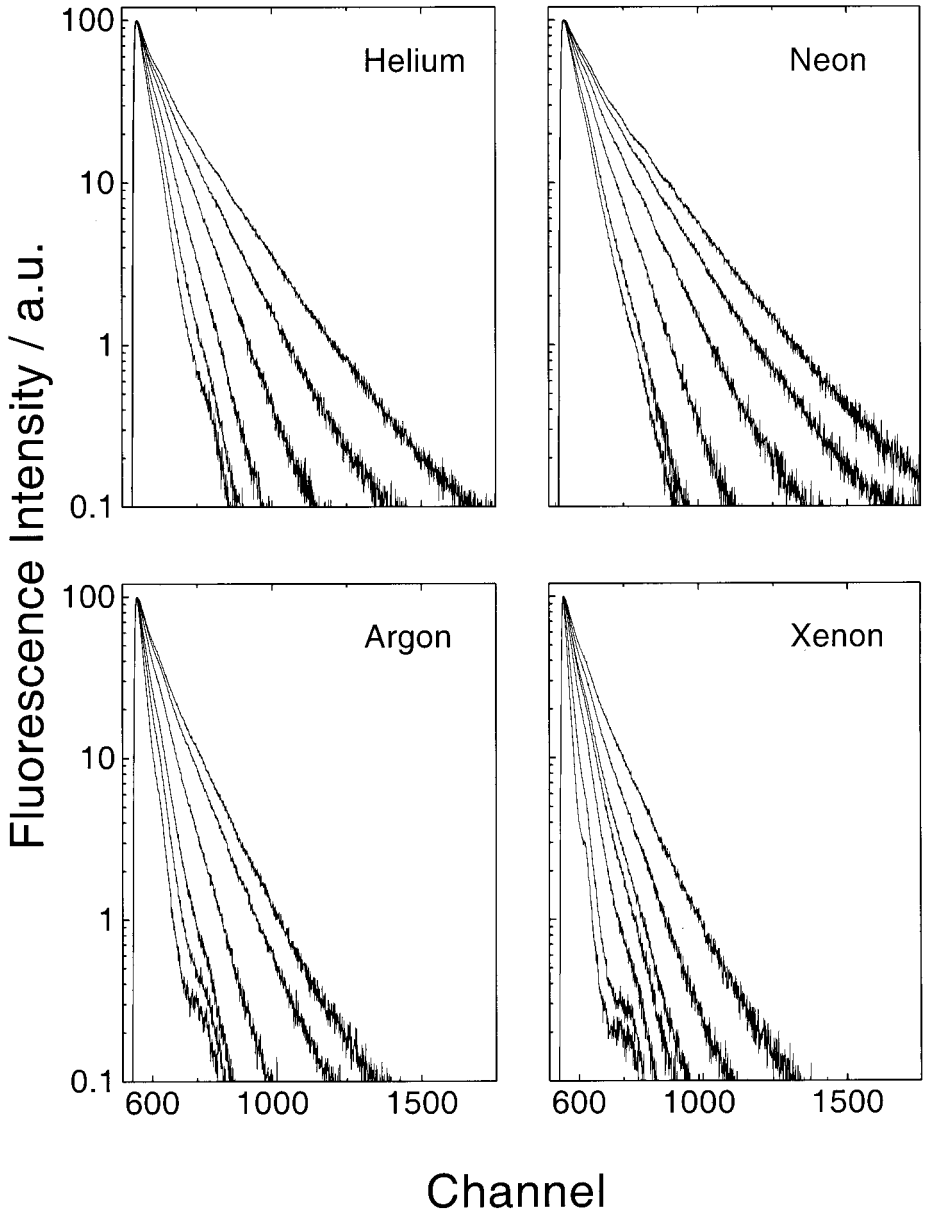

Figure 4. Pressure dependence of fluorescence decay curves of *trans*-stilbene at 323 K in noble bath gases. Semilogarithmic plots of normalized number of fluorescence photons versus channel number are shown for different pressures as given in bar from top to bottom trace as follows: helium (1, 2, 4, 8, 14, 20); neon (0.5, 1, 2, 4, 8, 10); argon (0.7, 1, 2, 4, 6, 10); xenon (0.3, 0.5, 0.8, 1.5, 3, 6). The plots contain raw experimental data not corrected for instrument artifacts visible in the system response function.

and reaction:

$$\frac{dg(E,t)}{dt} = Z\int_0^\infty P(E,E')\,g(E',t)dE' - Zg(E,t) - k_f(E)\,g(E,t) \quad (4)$$

where $g(E,t)$ = vibrational energy distribution at time t, Z = pressure dependent collision frequency, and $P(E,E')$ = collisional transition probability from energy E' to E). The numerical solution of this equation requires specification of the functional form of the collisional transition probability $P(E,E')$. A simple exponential down model was used in this work. For downward collisions one assumes

$$P(E,E') = C(E')\exp\left(\frac{E-E'}{\alpha(E')}\right) \quad E < E' \quad (5)$$

where the efficiency of collisional energy transfer is characterized by the parameter $\alpha(E)$, which is equivalent to the average energy transferred per downward collision $<\Delta E_{down}>(E)$. The corresponding probability for upward collisions is given by detailed balancing:

$$P(E,E') = C(E')\frac{f(E)}{f(E')}\exp\left(\frac{E'-E}{\alpha(E')}\right) \quad E' < E \quad (6)$$

where $f(E)$ denotes the thermal equilibrium distribution of vibrational energy.

The normalization constants $C(E)$ in eqs 5 and 6 were calculated by numerical solution of the integral equation[46]

$$C(E) = \int_0^\infty \exp\left(\frac{E-E'}{\alpha(E)}\right)dE \Big/ \left(1 - \frac{1}{f(E)}\int_E^\infty \frac{f(E')}{C(E')}\exp\left(\frac{E'-E}{\alpha(E)}\right)dE\right) \quad (7)$$

The choice of the functional form for the transition probability $P(E,E')$ is justified by earlier master equation simulations showing that macroscopic kinetics are insensitive to the details

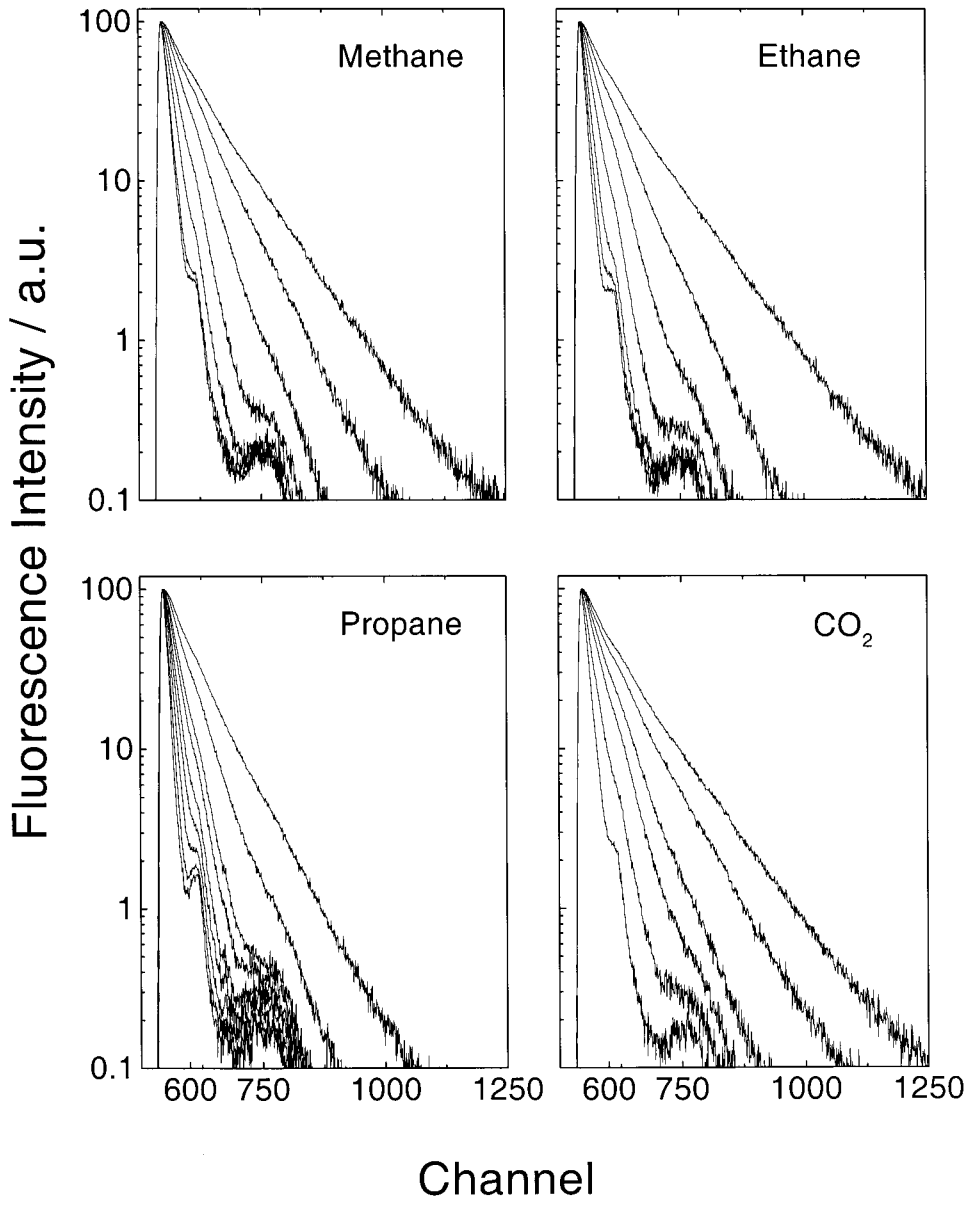

Figure 5. Pressure dependence of fluorescence decay curves of *trans*-stilbene at 323 K in noble bath gases. Semilogarithmic plots of normalized number of fluorescence photons versus channel number are shown for different pressures as given in bar from top to bottom trace as follows: methane (0.5, 1, 2, 4, 8, 16, 20); ethane (0.2, 0.5, 1, 2, 4, 10); propane (0.2, 0.4, 1, 2, 3, 5); CO_2 (0.3, 0.5, 1, 1.5, 3, 8). The plots contain raw experimental data not corrected for instrument artifacts visible in the system response function.

of the transition probability function $P(E,E')$ and are determined almost entirely by the average energy transferred per collision $<\Delta E(E)>$ and by $<\Delta E^2(E)>$.[47] This conclusion most probably will also hold at the levels of vibrational excitation present in our experiments, as a recent detailed comparison of equilibrium and nonequilibrium simulations of vibrational energy transfer of azulene in CO_2 indicates.[48−50] We also would like to stress at this point that the choice of collision model we use to describe the energy transfer contribution to the observed kinetics does not have a significant influence on the overall analysis of the experimental data.

For numerical solution of eq 4, vibrational energy levels were grouped into discrete intervals $E_i < E < E_i + \delta E$ such that the partial differential equation is transformed into a set of linear differential equations:

$$\frac{dg(E_i)}{dt} = Z\sum_k P(E_i,E_k)g(E_k) - Zg(E_i) - k_f(E_i)g(E_i) \quad (8)$$

A grain size of 50 cm^{-1} was found to be sufficient for our simulations. The numerical integration of eq 7 was performed by Gear's method of backward differentiation using routines from the IMSL subroutine library.[51]

Collision frequencies Z are considered to be independent of energy in this approach and represented by the Lennard-Jones value Z_{LJ}, which is calculated as previously[14] using the parameters listed in Table 1.

Pressure Dependence of Fluorescence Decays. The single-exponential part of the fluorescence decay curves at longer times reflects the decay out of the stationary distribution $g'(E)$ maintained by collisional energy transfer between *trans*-stilbene and the bath gas, which differs significantly from the initially prepared distribution $g(E,t=0) = f(E)$ as illustrated in Figure 7. Modeling this part of the decay, therefore, yields the parameter $\alpha(E)$ characterizing the collisional transition probability $P(E,E')$. Because of the limited energy range it is sufficient to regard α as energy independent when performing the master equation simulations. Comparing experimental fluorescence decays and

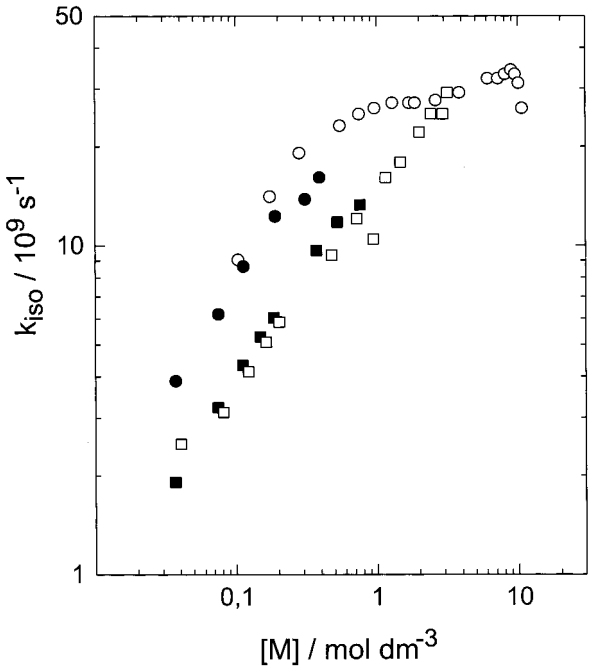

Figure 6. Density dependence of first-order photoisomerization rate constants k_{iso} of *trans*-stilbene; bath gas ethane at 323 K from single-exponential part of decay, this work (●); ethane at 350 K (○);[31] methane at 323 K from single-exponential part of decay, this work (■); methane at 296 K (□).[39]

simulated curves at pressures well below 1 bar, we obtained values of α for the different bath gases as listed in Table 1. As illustrated in Figure 8, the accuracy of the optimized values for α is better than 5%. They increase with collider mass and polarizability as observed in other studies, though the absolute values are somewhat higher than one would expect by comparison with energy transfer from other molecules such as, e.g., azulene or cycloheptatriene in their electronic ground state.[52−54]

In the pressure range above 1 bar, using the energy transfer parameters α determined for the various bath gases, one should be able to model the variation of the measured fluorescence decays with increasing pressure without any additional adjustments. However, as illustrated in Figure 9 for the bath gas argon at pressures of 0.5 and 10 bar, this is not the case. Instead, in all bath gases we observe a significant enhancement of the decay rate in this pressure regime surpassing that predicted by collisional energy transfer. A small effect even is found for the weakest collider helium. Already in this low-density regime, therefore, the bath gas has a noticeable effect in addition to its role as a heat bath. In principle, all input parameters in the master equation could be considered as possible sources of a hidden pressure dependence.

The initial distribution $g(E,t=0) = f(E)$ was found to be consistent with the observed decay under collision-free conditions and would not be expected to change with pressure. As the bathochromic solvent shift of the electronic absorption spectrum is negligibly small in this density range,[14,28] it does not lead to a significant change of the excess energy in the excited state.

A dependence of the collisional energy transfer probability as characterized by α on density in the gas phase has not been observed yet and would seem extremely unlikely in this pressure range. There is strong evidence from other experimental studies[52,55] that it does not change over a wide density range approaching even liquid-like densities. In any case, a change in the energy transfer mechanism and hence $P(E,E')$ would not be expected to occur at the low densities investigated here.[56]

Energy transfer is still in the binary collision regime, but the effective collision frequency may differ from the Lennard-Jones collision number Z_{LJ} due to enhanced local density in the vicinity of the solute.[52] The estimate of the magnitude of the enhancement of the collision rate based on other experimental systems,[52,53,55] however, is considerably smaller than the observed acceleration of the fluorescence decays, so its contribution may be neglected in the discussion.

Microcanonical specific rate coefficients $k(E)$ could change with density, if the effective PES for the reaction is altered already at low bath gas pressures by solvent−solute interactions. Such an assumption extends our earlier hypothesis[18] about the solvent density influence on the PES to environments of considerably lower density.

The pressure effect on $k(E)$ is also clearly visible in the initial parts of the fluorescence decays as illustrated in Figure 10. As the initial distribution prepared by excitation of the 0−0 transition to the S_1 state is the thermal distribution at 323 K, immediately after excitation the fluorescence should decay with a rate corresponding to the high-pressure limit of the unimolecular rate coefficient

$$k_\infty = \int_{E_0}^{\infty} k(E) f(E)\, \mathrm{d}E \qquad (9)$$

independent of bath gas pressure. The measured decay traces, in contrast, show an acceleration also of the initial rate with pressure, a clear indication that interaction with bath gas molecules leads to " static" effects beyond collisional energy transfer.

Consequently, we modify the master equation approach to include "static" bath gas effects by ad hoc introduction of a pressure-dependent $k(E)$ by taking the potential energy barrier E_0 as an adjustable parameter in our numerical simulations; i.e., for every decay trace we vary E_0 and calculate a new set of $k(E)$ until we obtain agreement between the simulated curve, convoluted with the appropriate system response function, and the measured fluorescence decay trace. Initial distribution, collision frequency and energy transfer parameter α are kept fixed during this final stage of the simulation procedure. The sensitivity of the simulated curves to changes in E_0 is illustrated in Figure 11, showing that the accuracy of the fitted barrier heights is about 1% for a single trace. Fitted values of E_0 at 10 bar obtained in this way are listed in Table 1.

Discussion

Low-Pressure Limit. In the low pressure limit the rate of a unimolecular reaction is controlled by collisional activation only and depends, therefore, linearly on the rate of binary collisions which is proportional to the bath gas pressure, such that $k_{iso}(p) = k_0 p$; the linearity with pressure is considered as a signature of the low-pressure limit. In the case of *trans*-stilbene, however, identifying this regime is complicated by the additional gas bath effects that lead to an increase of the rate coefficient. Only at pressures below about 1 bar does the pressure dependence of k_{iso} reflect almost exclusively the increase in collision rate, and one may extract k_0 from the slope of the linear part of the curves shown in Figure 12. In this way one finds the low-pressure limit at an order of magnitude lower density than assumed previously.[28] Values of k_0 for the various gases are given in Table 1. The pressure dependence of the rate coefficient toward higher pressures as displayed in Figure 6 is a superposition of the

TABLE 1: Lennard-Jones Parameters, Optimized Energy Transfer Parameters, α, Low-Pressure Limit Rate Constants, k_0, and Optimized Barrier Heights, E_0, at $p = 10$ Bar for the Bath Gases Used in This Study

bath gas	σ_{LJ} [nm] [a]	ϵ_{LJ}/k_B [K][a]	α [cm^{-1}] ($E = 2194$ cm^{-1})	k_0 [10^9 s^{-1} bar^{-1}]	E_0 [cm^{-1}] ($p = 10$ bar)
He	0.2551	10.22	130	0.47	1175
Ne	0.2820	32.8	200	0.74	1120
Ar	0.3542	93.3	320	1.49	1110
Xe	0.4047	231.0	430	2.58	900 ($p = 6$ bar)
N_2	0.3798	71.4	340	1.40	1000
CO_2	0.3914	195.2	500	3.40	950 ($p = 7$ bar)
CHF_3	0.44	184	950	5.62	900 ($p = 7$ bar)
CH_4	0.3758	148.6	330	1.75	990
C_2H_6	0.4443	215.7	510	4.15	900
C_3H_8	0.5118	237.1	860	7.10	850 ($p = 7$ bar)
trans-stilbene	0.78	651			1250 ($p = 0$)

[a] Data from Reid, R. C.; Prausnitz, J. M.; Poling, B. E. *The Properties of Gases and Liquids*, 4th ed.; McGraw Hill: New York, 1987.

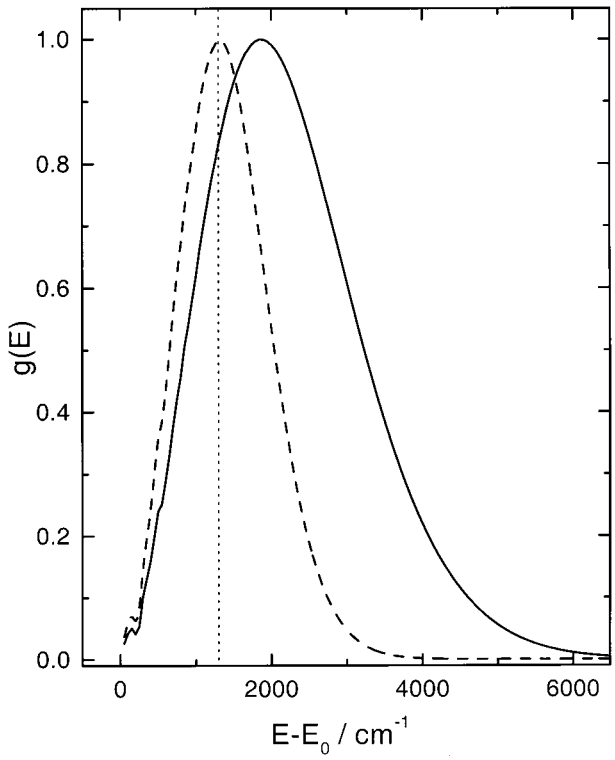

Figure 7. Initially prepared vibrational distribution $g(E,t=0) = f(E)$ (solid curve) and stationary distribution $g'(E)$ at $T = 323$ K (dashed curve) and $p = 0.5$ bar in neon. Dotted line indicates position of barrier.

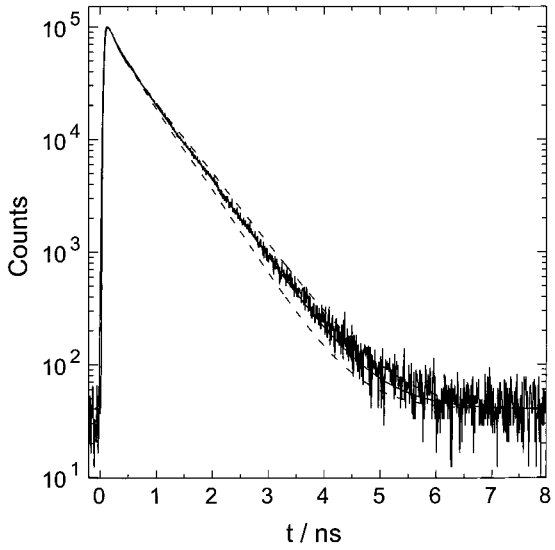

Figure 8. Sensitivity of master equation simulations to changes in the energy transfer parameter α. The measured trace is for methane at 323 K and 0.5 bar. The solid line merging with the signal trace is the simulated signal using the optimized value of α = 330 cm^{-1}; the dashed lines above and below correspond to values of α 10% smaller and higher, respectively.

conventional falloff effect and the additional bath gas influence on $k(E)$ as discussed below.

High-Pressure Limit. The numerical simulation of the pressure dependence of the fluorescence decays implies the interpretation that specific interactions between *trans*-stilbene and each bath gas lead to specific changes in the effective barrier of reaction as the local excess density in the vicinity of *trans*-stilbene increases with rising pressure. The results of our simulation, therefore, can be summarized in Figure 13, which shows the pressure-dependent decrease of effective barrier heights $E_0(p)$ for the bath gases investigated in this study. The curves are distinct for each bath gas and approach-specific solvent dependent limiting values as the pressure approaches the 10^1 bar range. The equivalent effect, obviously, appears in the high-pressure limit k_∞ of the rate coefficient which can be calculated from eq 9 using $E_0(p)$ and $k(E;p)$ obtained from the simulations. The rate coefficients obtained in this way equal initial fast decay rate constants that can be extracted from the fluorescence decays directly by using convolution and fitting techniques. The pressure-dependent $k_\infty(p)$ shown in Figure 14 consequently tends to reach a bath gas specific plateau at higher pressures.

Analyzing the bath gas dependence of $k_\infty(p)$ two general observations can be made: (i) bath gases with higher polarizability display a larger slope of $k_\infty(p)$ and (ii) also lead to a higher plateau value of $k_\infty(p)$ at higher pressures of the order of 10 bar.

Observation (i) is qualitatively consistent with all proposed models, as increasing the collision efficiency of the collider would enhance collision induced IVR (model I),[22,23,57−59] vibrational cooling (model II/iii),[27] effective barrier lowering (model II/ii),[18] and curve crossing efficiency (model II/i).[26] For the latter model, however, a transition from a nonadiabatic reaction to an adiabatic process in this density regime seems rather unlikely, as a substantial slow-down of passage through the curve crossing region is not to be expected in this pressure range.

In contrast, observation (ii) is not in agreement with predictions of models (I), (II/i), and (II/iii) which predict the same plateau value of $k_\infty(p)$ for all bath gases. On the other hand, it is consistent with our proposition of a density-dependent effective barrier of reaction which is explicitly expected to attain a solvent specific value at higher pressures. The $E_0(p)$ are in close agreement with effective barrier heights obtained from

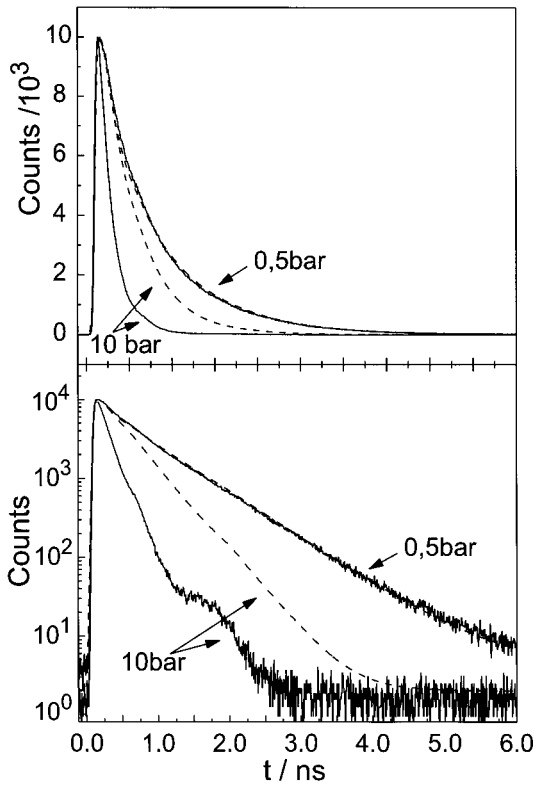

Figure 9. Fluorescence decays of *trans*-stilbene in argon at 353 K and pressures of 0.5 bar (upper full line) and 10 bar (lower full line). The dashed curves are from the corresponding master equation simulations using the energy transfer parameter α obtained from fitting the simulations to experimental decays at $p \leq 0.5$ bar.

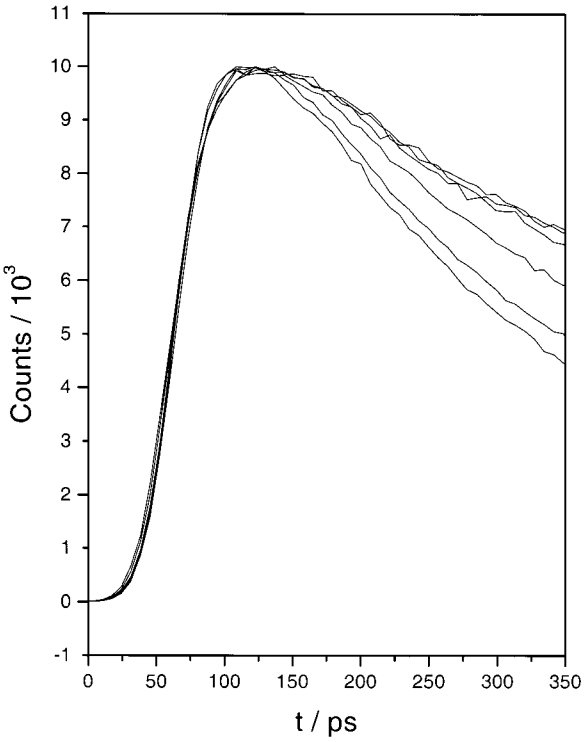

Figure 10. Initial fluorescence decay period of *trans*-stilbene in neon bath gas at pressures (from top to bottom) of 0.5, 1, 2, 4, 8, and 10 bar at 323 K, illustrating the acceleration of the initial decay rate with increasing pressure.

pressure- and temperature-dependent measurements at higher pressures and in compressed liquids using ps-pump−probe spectroscopy.[14,18,28,29,60−63]

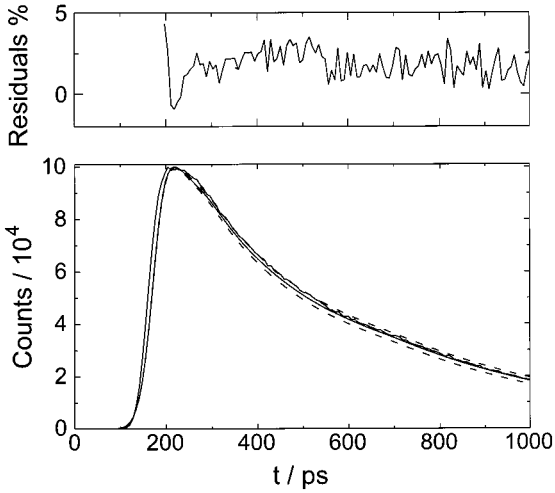

Figure 11. Sensitivity of master equation simulations to changes in the barrier height E_0. The measured trace is for neon at 323 K and 4 bar. The solid line merging with the signal trace is the simulated signal using the optimized value of $E_0 = 1175$ cm^{-1}, the dashed lines above and below correspond to values of E_0 15 cm^{-1} higher and smaller, respectively. At the top, the relative residuals of the optimized simulation are shown.

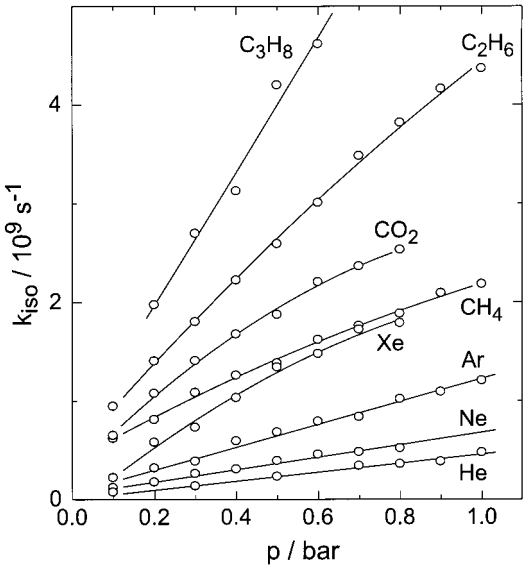

Figure 12. Low-pressure regime of photoisomerization of *trans*-stilbene in different gases. Pressure dependence of k_{iso} at 323 K up to $p = 1$ bar in helium, neon, argon, xenon, CO_2, methane, ethane, and propane, as indicated.

The question remains whether one can explain the magnitude of the bath gas influence on the effective barrier height ranging from −75 cm^{-1} in He to about −400 cm^{-1} in propane entirely in terms of a "static" barrier shift. Without reliable knowledge of the excited state PES one can only speculate about its properties in the barrier region. We have indications from earlier pump−probe absorption studies in polar solvents that *trans*-stilbene in the S_1 state in the vicinity of the barrier may possess an appreciable dipole moment,[62,63] which may interact with polarizable bath gas molecules. To estimate the magnitude of the effect one has to know the intermolecular well depth for the binary bath gas−*trans*-stilbene interaction. A promising method to determine these well depths is the analysis of pressure-dependent spectral shift data in supercritical solvents.[55,64] A study of *trans*-stilbene in Xenon [65] gives a Lennard-Jones well depth of 475 cm^{-1} at a pressure of 6 bar. From the radial distribution function calculated for this pressure one finds

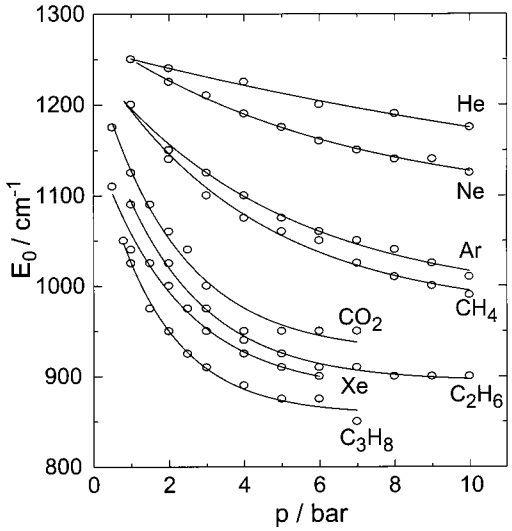

Figure 13. Pressure dependence of optimized barrier heights $E_0(p)$ in the bath gases in helium, neon, argon, xenon, CO_2, methane, ethane, and propane, as indicated.

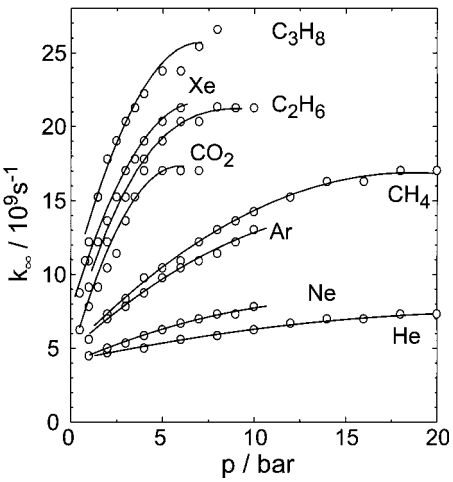

Figure 14. Pressure dependence of the "high-pressure limit" of the rate coefficient $k_\infty(p)$ in the bath gases in helium, neon, argon, xenon, CO_2, methane, ethane, and propane, as indicated.

an average local density enhancement equivalent to about 0.8 Xe atom at contact distance with a stilbene molecule. Using the polarizability volume of Xe (4.02×10^{-30} m^3) and a Lennard-Jones radius $\sigma_{\text{stilbene-Xe}} = 0.55$ nm together with a dipole moment of *trans*-stilbene in the barrier region of $\mu = 20 \times 10^{-30}$ Cm estimated in our previous studies, one obtains a reduction of the height of the potential energy barrier of about 100 cm^{-1}, which is about a third of the value listed in Table 1. One arrives at similar contributions of the "static" barrier shift for the other bath gases, if one estimates well depths on the basis of data obtained for azulene.[55,64] The overall picture that evolves from these considerations is that the pressure-dependent effective barrier height definitely contains a solvent specific substantial "static" contribution causing the bath gas-dependent limiting values of $E_0(p)$.

The quantitative analysis presented above obviously depends on the choice of the sets of vibrational frequencies of *trans*-stilbene in the S_1 and the transition state that one uses to calculate microcanonical rate constants $k(E)$ and vibrational distributions. Obviously, the observed $k(E)$ of the jet-cooled, isolated molecule can be fit by any model as long as the ratios $W^{\ddagger}(E)/\rho(E)$ remain unchanged. In this sense, RRKM-modeling does not provide a means to determine "correct" frequencies

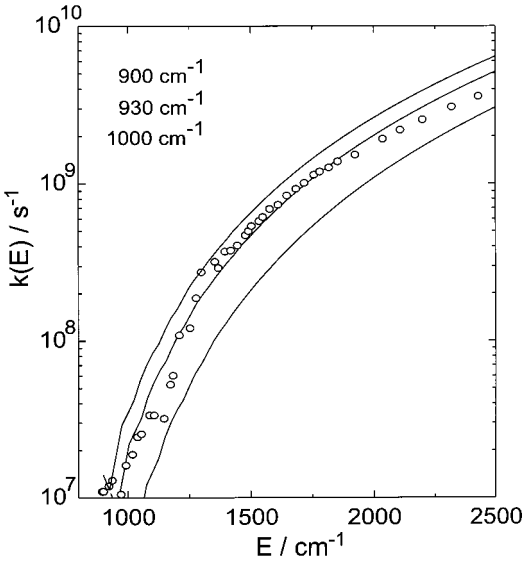

Figure 15. RRKM fit to experimental $k(E)$ measured in the supersonic jet[21] using the Vachev, Gershinsky, Pollak potential model[67] and barrier heights E_0 of 900, 930, and 1000 cm^{-1}, from top to bottom.

and one may use scaling factors instead without any loss of rigor. Such scaling factors would also take care of any anharmonicity effects that might be present. Having chosen a model to represent measured $k(E)$ data, one has to go one step further and try to describe the measured fluorescence decay under collision-free conditions under thermal conditions by defining a reasonable initial distribution. This can be done equally well using the Warshel−Troe or the Negri−Orlandi set of vibrational frequencies by assuming an initial Boltzmann distribution in the S_1 state. The discrepancy with experiment then arises if one calculates k_∞, as discussed at length in the preceding sections. Gershinsky and Pollak[27]proposed an alternative approach and used frequencies obtained from a potential model of *trans*-stilbene by Vachev et al.[66,67] Their model gives a considerably higher density of states due to a higher number of low-frequency vibrations, i.e., 3×10^7/cm^{-1} at 2200 cm^{-1} and 4×10^5/cm^{-1} at 1260 cm^{-1}. However, as demonstrated in Figure 15, fitting their model to the measured $k(E)$ values gives a value for the barrier of reaction in the isolated molecule of $E_0 = (930 \pm 30)$ cm^{-1}.[21] This value is significantly lower than the commonly accepted value of (1250 ± 50) cm^{-1}.[21,23,24,35]

Obviously, in the framework of this model, taking the initial distribution to be the Boltzmann distribution at 323 K, one cannot reproduce the observed decay in pure *trans*-stilbene vapor. Gershinsky and Pollak therefore assumed that the optical excitation from the S_0 to the S_1 state is accompanied by vibrational cooling due to variations in Franck−Condon factors. Assuming that the distribution can still be defined by a single vibrational temperature, one finds that with $T = 208$ K one obtains agreement with measured decay as shown in Figure 16. A change in the excitation wavelength would involve different Franck−Condon factors for optical excitation, and one would expect to create a different initial distribution in the S_1 state. Fluorescence decays in *trans*-stilbene vapor at 323 K measured in our laboratory with 290 nm excitation, however, could be simulated using our model and the unaltered initial distribution, i.e., the thermal distribution of the ground state carried by optical excitation with the corresponding excess excitation energy into the S_1 state. This experimental observation would be highly surprising if vibrational Franck−Condon cooling was effective.

Addition of a bath gas will then cause this cold initial distribution to evolve toward the bath temperature stationary

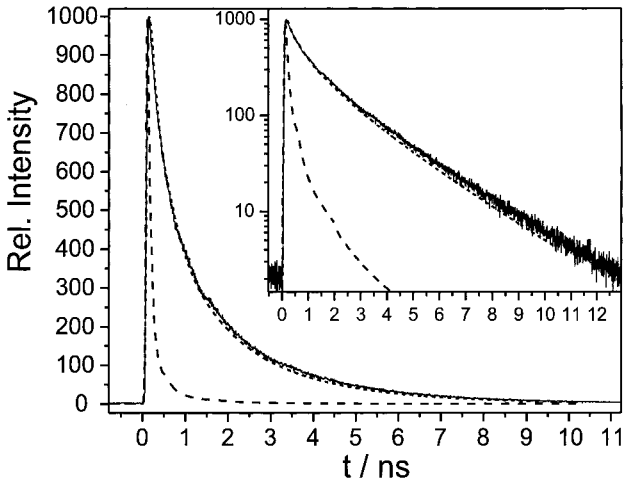

Figure 16. Comparison of vibrational cooling in the Vachev, Gershinsky, Pollak potential model[67] with experimental fluorescence decay in *trans*-stilbene vapor measured at 323 K: measured decay trace (−); simulated trace with initial distribution taken as thermal distribution at 323 K (− − −), and at 208 K (- - -).

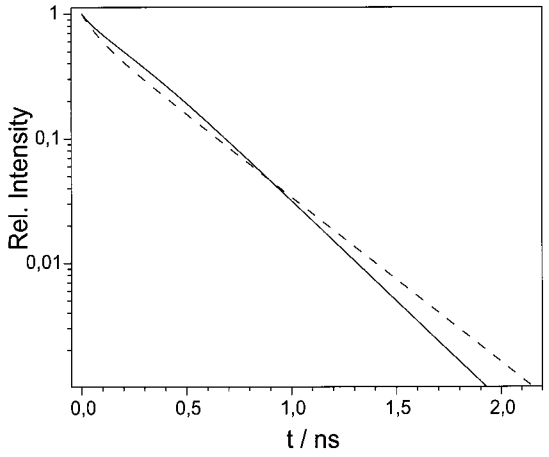

Figure 17. Numerical master equation simulations of fluorescence decays of *trans*-stilbene in nitrogen at 2 bar and 323 K following excitation at 310.4 nm: according to barrier shift model using an initial distribution equal to the thermal vibrational distribution at the temperature of the bath (− − −), which exactly reproduces the experimentally measured curve; and according to the model of Gershinsky and Pollak using an initial vibrational distribution corresponding to a temperature of 208 K (−).

distribution corresponding to the particular pressure. This means that the initial period of the decay will be slower, due to the lower temperature, and there will be an acceleration of the decay at later times, because the bath gas heats the *trans*-stilbene molecule before it reaches the stationary regime. In Figure 17 we demonstrate this effect by comparing master equation simulations for our model, which is in perfect agreement with the experimental decay, and for the model proposed by Pollak and Gershinsky. The simulation performed on the basis of the latter model is qualitatively different from the observed decay which is a clear indication that vibrational Franck−Condon cooling with subsequent heating is not taking place.

Conclusion

A systematic experimental study of the bath gas and pressure dependence of the photoisomerization of *trans*-stilbene in the low to intermediate pressure regime and its detailed numerical simulation by a master equation reveals specific bath gas effects that are already observable at pressures of about 1 bar. The low-pressure regime of the unimolecular reaction in the S_1 state is located in the pressure range well below 1 bar for most of the bath gases. The effective "high pressure limit" of the photoisomerization rate constant k_∞ that can be extracted from the simulation in our experiments is found to be pressure dependent approaching a bath gas specific plateau value in the 10 bar range for bath gases as methane, ethane, propane, or xenon.

Of the models proposed so far, only the assumption of a solvent-specific density-dependent effective barrier height $E_0(p)$ can explain the observation of a bath gas dependent limiting value for $k_\infty(p)$, a conlusion that is independent of the details of the potential model used for *trans*-stilbene or the collisional model employed in master equation simulations. The values obtained for $E_0(p)$ agree with the trend observed in earlier experiments in highly compressed gases and liquids. An additional contribution from collision-induced IVR to the observed enhancement of the rate coefficient with increasing pressure, however, cannot be ruled out, although observed IVR times[68] seem to indicate that in a molecule of this size it is rather unlikely that IVR at low pressures is a rate determining step in the dynamics of the reaction. This point, however, is still under discussion and has to be pursued further.[58,59]

The proposition of a different potential model for *trans*-stilbene together with the effect of vibrational Franck−Condon cooling is not consistent with our measured fluorescence decays, because it would lead to qualitatively different shapes of the fluorescence decay curves which would be clearly visible in the experiment. Furthermore, the fluorescence emission spectrum of *trans*-stilbene vapor at different excitation wavelengths does not show any noticeable changes of spectral shape that would be expected if Franck−Condon factors would affect the initial distribution in the excited state.[69] Also, there is no spectral evolution in the fs time-resolved stimulated emission spectrum within the first 100 fs in liquid solution that would be indicative of any such effect.[70]

Acknowledgment. We thank Martin Votsmeier for many discussions and much help in the initial stages of the project. Financial assistance by the Deutsche Forschungsgemeinschaft in the framework of the Sonderforschungsbereich 357 *Molekulare Mechanismen unimolekularer Prozesse* and the Graduiertenkolleg *Kinetik und Selektivität chemischer Prozesse in verdichteter fluider Phase* is gratefully acknowledged.

References and Notes

(1) Allen, M. T.; Whitten, D. G. *Chem. Rev.* **1989**, *89*, 1691−1702.
(2) Saltiel J.; Sun, Y.-P. *Photochromism, Molecules, and Systems*; Elsevier: Amsterdam, 1990; p 64.
(3) Görner, H.; Kuhn, H. J. *Adv. Photochem.* **1995**, *19*, 1.
(4) Fleming, G. R.; Courtney, S. H.; Balk, M. W. *J. Stat. Phys.* **1986**, *42*, 83−104.
(5) Waldeck, D. H. *Chem. Rev.* **1991**, *91*, 415.
(6) Waldeck, D. H. *J. Mol. Liq.* **1993**, *57*, 127−148.
(7) Fleming, G. R.; Hänggi, P. *Activated Barrier Crossing*; World Scientific: Singapore, 1993.
(8) Voth, G. A.; Hochstrasser, R. M. *J. Phys. Chem.* **1996**, *100*, 13034−13049.
(9) Velsko, S. P.; Fleming, G. R. *J. Chem. Phys.* **1982**, *76*, 3553−3562.
(10) Rothenberger, G.; Negus, D. K.; Hochstrasser, R. M. *J. Chem. Phys.* **1983**, *79*, 5360−5367.
(11) Hynes, J. T. *J. Stat. Phys.* **1986**, *42*, 149−168.
(12) Agmon, N.; Kosloff, R. *J. Phys. Chem.* **1987**, *91*, 1988−1996.
(13) Park, N. S.; Waldeck, D. H. *Chem. Phys. Lett.* **1990**, *168*, 379−384.
(14) Schroeder, J.; Schwarzer, D.; Troe, J.; Voss, F. *J. Chem. Phys.* **1990**, *93*, 2393−2404.
(15) Courtney, S. H.; Kim, S. K.; Canonica, S.; Fleming, G. R. *J. Chem. Soc., Faraday Trans. 2* **1986**, *82*, 2065−2072.

(16) Lee, M.; Bain, A. J.; McCarthy, P. J.; Han, C. H.; Haseltine, J. N.; Smith, A. B., III; Hochstrasser, R. M. *J. Chem. Phys.* **1986**, *85*, 4341−4347.
(17) Sundström, V.; Gillbro, T. *Chem. Phys. Lett.* **1984**, *109*, 538−543.
(18) Schroeder, J.; Troe, J. *Chem. Phys. Lett.* **1985**, *116*, 453.
(19) Troe, J. *J. Phys. Chem.* **1986**, *90*, 357.
(20) Heikal, A. A.; Chong, S. H.; Baskin, J. S.; Zewail, A. H. *Chem. Phys. Lett.* **1995**, *242*, 380−389.
(21) Lienau, C.; Schroeder, J.; Troe, J.; Wack, K. *Ber. Bunsen-Ges. Phys. Chem.* **1997**, *101*, 614−624.
(22) Khundkar, L. R.; Marcus, R. A.; Zewail, A. H. *J. Phys. Chem.* **1983**, *87*, 2473−2476.
(23) Syage, J. A.; Felker, P. M.; Zewail, A. H. *J. Chem. Phys.* **1984**, *81*, 4706−4723.
(24) Majors, T. J.; Even, U.; Jortner, J. *J. Chem. Phys.* **1984**, *81*, 2330−2338.
(25) Troe, J. *Chem. Phys. Lett.* **1985**, *114*, 241−247.
(26) Felker, P. M.; Zewail, A. H. *J. Phys. Chem.* **1985**, *89*, 5402−5411.
(27) Gershinsky, G.; Pollak, E. *J. Chem. Phys.* **1996**, *105*, 4388−4390.
(28) Maneke, G.; Schroeder, J.; Troe, J.; Voss, F. *Ber. Bunsen-Ges. Phys. Chem.* **1985**, *89*, 896−906.
(29) Schroeder, J.; Troe, J.; Vöhringer, P. *Z. Phys. Chem.* **1995**, *188*, 287.
(30) Hänggi, P.; Talkner, P.; Borkovec, M. *Rev. Mod. Phys.* **1990**, *62*, 251 .
(31) Lee, M.; Holtom, G. R.; Hochstrasser, R. M. *Chem. Phys. Lett.* **1985**, *118*, 359−363.
(32) Kuharski, R. A.; Chandler, D.; Montgomery, J.; Rabii, F.; Singer, S. J. *J. Phys. Chem.* **1988**, *92*, 3261 .
(33) Syage, J. A.; Lambert, W. M.; Felker, P. M.; Zewail, A. H.; Hochstrasser, R. M. *Chem. Phys. Lett.* **1982**, *88*, 266−270.
(34) Amirav, A.; Jortner, J. *Chem. Phys. Lett.* **1983**, *95*, 295−300.
(35) Courtney, S. H.; Balk, M. W.; Philips, L. A.; Webb, S. P.; Yang, D.; Levy, D. H.; Fleming, G. R. *J. Chem. Phys.* **1988**, *89*, 6697−6707.
(36) Lienau, C. Ph.D. thesis, Universtät Göttingen, 1991.
(37) Greene, B. I.; Hochstrasser, R. M.; Weisman, R. B. *J. Chem. Phys.* **1979**, *71*, 544−545.
(38) Greene, B. I.; Hochstrasser, R. M.; Weisman, R. B. *Chem. Phys.* **1980**, *48*, 289−298.
(39) Balk, M. W.; Fleming, G. R. *J. Phys. Chem.* **1986**, *90*, 3975−3983.
(40) Meyer, A.; Schroeder, J.; Troe, J.; Votsmeier, M. *J. Photochem. Photobiol. A: Chem.* **1997**, *105*, 345−352.
(41) Courtney, S. H.; Fleming, G. R. *J. Chem. Phys.* **1985**, *83*, 215−222.
(42) Saltiel, J.; Waller, A. S.; Sears, D. F., Jr.; Garrett, C. Z. *J. Phys. Chem.* **1993**, *97*, 2516−2522.
(43) Beyer, T.; Swinehart, D. F. *Comm. Ass. Comput. Mach.* **1973**, *16*, 2473.
(44) Astholz, D. C.; Troe, J.; Wieters, W. *J. Chem. Phys.* **1979**, *70*, 5107.
(45) Negri, F.; Orlandi, G. *J. Phys. Chem.* **1991**, *95*, 748−757.
(46) Gilbert, R. G.; Luther, K.; Troe, J. *Ber. Bunsen-Ges. Phys. Chem.* **1983**, *87*, 169−177.
(47) Troe, J. *J. Phys. Chem.* **1983**, *87*, 1800−1804.
(48) Heidelbach, C.; Vikhrenko, V.; Schwarzer, D.; Schroeder, J. *J. Chem. Phys.* **1999**, *110*, 5286.
(49) Heidelbach, C.; Vikhrenko, V.; Schwarzer, D.; Fedchenia, I. I.; Schroeder, J. *J. Chem. Phys.* **1999**, *111*.
(50) Vikhrenko, V.; Heidelbach, C.; Schwarzer, D.; Nemtsov, V. B.; Schroeder, J. *J. Chem. Phys.* **1999**, *110*, 5273.
(51) IMSL. Interactive Productivity Tools, FORTRAN/Math/Library. Visual Numerics Inc.: Houston, 1995.
(52) Schwarzer, D.; Troe, J.; Votsmeier, M.; Zerezke, M. *J. Chem. Phys.* **1996**, *105*, 3121−3131.
(53) Benzler, J.; Linkersdörfer, S.; Luther, K. *J. Chem. Phys.* **1997**, *106*, 4992−5005.
(54) Shi, J.; Barker, J. R. *J. Chem. Phys.* **1988**, *88*, 6219−6227.
(55) Schwarzer, D.; Troe, J.; Zerezke, M. *J. Phys. Chem. A* **1998**, *102*, 4207−4212.
(56) Heidelbach, C.; Schroeder, J.; Schwarzer, D.; Vikhrenko, V. *Chem. Phys. Lett.* **1998**, *291*, 333.
(57) Nordholm, S. *Chem. Phys.* **1989**, *137*, 109−120.
(58) Bolton, K.; Nordholm, S. *Chem. Phys.* **1996**, *203*, 101−126.
(59) Leitner, D. N.; Wolynes, P. G. *Chem. Phys. Lett.* **1997**, *280*, 411−418.
(60) Schroeder, J. *Ber. Bunsen-Ges. Phys. Chem.* **1991**, *95*, 233.
(61) Schroeder, J.; Troe, J.; Vöhringer, P. *Chem. Phys. Lett.* **1993**, *203*, 255.
(62) Schroeder, J.; Schwarzer, D.; Troe, J.; Vöhringer, P. *Chem. Phys. Lett.* **1994**, *218*, 43.
(63) Mohrschladt, R.; Schroeder, J.; Schwarzer, D.; Troe, J.; Vöhringer, P. *J. Chem. Phys.* **1994**, *101*, 7566.
(64) Schwarzer, D.; Troe, J.; Zerezke, M. *J. Chem. Phys.* **1997**, *107*, 8380−8390.
(65) Schroeder, J.; Schwarzer, D., to be published.
(66) Vachev, V. D.; Frederick, J. H.; Grishanin, B. A.; Zadkov, V. N.; Koroteev, N. I. *J. Phys. Chem.* **1995**, *99*, 5247.
(67) Gershinsky, G.; Pollak, E. *J. Chem. Phys.* **1997**, *107*, 812−824.
(68) Baskin, J. S.; Banares, L.; Pedersen, S.; Zewail, A. H. *J. Phys. Chem.* **1996**, *100*, 11920−11933.
(69) Rupp. L.; Schroeder, J.; Troe, J., to be published.
(70) Kovalenko, S.; Ruthmann, J.; Schroder, J., to be published.